

Electron spin manipulation and resonator readout in a double quantum dot nano-electromechanical system

N. Lambert

*Department of Basic Science, University of Tokyo, Komaba, Meguro-ku, Tokyo 153-8902, Japan**

I. Mahboob

NTT Basic Research Laboratories, NTT Corporation, Atsugi-shi, Kanagawa 243-0198, Japan

M. Pioro-Ladrière

Quantum Spin Information Project, ICORP, Japan Science and Technology Agency, Atsugi-shi, Kanagawa 243-0198, Japan

Y. Tokura

*NTT Basic Research Laboratories, NTT Corporation, Atsugi-shi, Kanagawa 243-0198, Japan and
Quantum Spin Information Project, ICORP, Japan Science and Technology Agency, Atsugi-shi, Kanagawa 243-0198, Japan*

S. Tarucha

*Department of Applied Physics, University of Tokyo,
Hongo, Bunkyo-ku, Tokyo, 113-0033, Japan and
Quantum Spin Information Project, ICORP, Japan Science and Technology Agency, Atsugi-shi, Kanagawa 243-0198, Japan*

H. Yamaguchi

*NTT Basic Research Laboratories, NTT Corporation, Atsugi-shi, Kanagawa 243-0198, Japan and
Department of Physics, Tohoku University, Sendai, Miyagi 980-8578, Japan*

Magnetically coupling a nano-mechanical resonator to a double quantum dot confining two electrons can enable the manipulation of a single electron spin and the readout of the resonator's natural frequency. When the Larmor frequency matches the resonator frequency, the electron spin in one of the dots can be selectively flipped by the magnetised resonator. By simultaneously measuring the charge state of the two-electron double quantum dots, this transition can be detected thus enabling the natural frequency of the mechanical resonator to be determined.

I. INTRODUCTION

Nano-electromechanical systems (NEMSs) enable the coupling of electronic and mechanical degrees of freedom^{1,2,3} and provide an arena in which quantum mechanical behaviour can be identified on macroscopic scales^{1,2,3,4,5,6}. A key requirement for the realization of quantum electromechanical systems is the efficient transduction of the miniscule displacements of the mechanical element. Meanwhile theoretical studies have proposed coupling NEMSs to quantum two-level systems realised in a variety of physical systems^{7,8,9,10}. The coupled system can potentially enable the implementation of protocols similar to those realised in cavity QED and on-chip circuit QED with superconducting qubits and transmission lines¹¹. Furthermore, manipulating a two-level system via NEMSs has the advantage that a change in its state can be used to distinguish between resonance and off resonance conditions of the mechanical element with great sensitivity.

In this work we present a proposal for coupling a NEM system to the spin of an electron in a double quantum dot (QD). Quantum dots are artificial structures which enable the confinement of a few or even one electron^{12,13,14}. In this regime, the spin of the individual electron forms a natural two-level system and provides great potential

for the realization of a solid-state qubit¹⁵. However, for a QD based spin qubit to be realized requires precise control and manipulation of the electron spins. Recently, coherent spin manipulation in a double quantum dot was demonstrated by rapid electrical control of the exchange interaction¹⁶ and by generating a local electron spin resonance (ESR) magnetic field¹⁷.

Here we describe how to exploit the versatility of a double quantum dot in order to realize an electron spin in a well defined state which is then coupled and controllably manipulated by the nano-mechanical resonator. Previously, coupling spin to a mechanical resonator has been both theoretically and experimentally considered^{18,19}; but the motivation of these studies was spin detection rather than spin manipulation. In the present scheme, the magnetised resonator selectively flips one of the two confined electron spins in the double dots (DDs) where the ESR field is produced by the oscillations of the magnetised resonator. The corresponding change in the two electron spin state is then detected by spin blockade charge sensing at the DDs. Concurrently, this also enables the resonator's natural frequency to be measured. As demonstrated in refs.^{16,17}, spin-blockade readout does not rely on large Zeeman fields as in the case of a single quantum dot²⁰ which is an important criterion for frequency matching between the electron spin and the

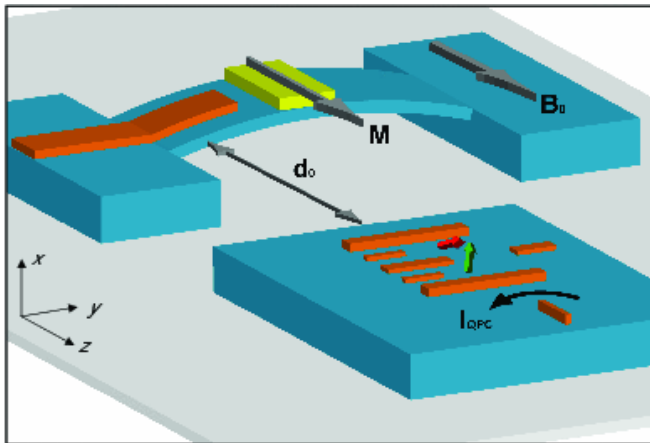


FIG. 1: (colour on-line) A schematic of the proposed coupled mechanical resonator double QD system. The mechanical oscillator is a suspended doubly clamped beam located a distance, d_0 , from the mesa on which the double QDs are defined via electrostatic gates (orange). The beam is actuated to resonance via the piezoelectric effect between the top gate, located at where the beam is clamped (orange), and the shallow buried 2DEG. A micro-magnet (yellow) of magnetisation, M , is incorporated onto the beam oscillator and moves in unison with the out of plane beam motion. The mechanical oscillator couples to the confined electron spins (red and green arrows) in the doubles QDs via the micro-magnet's stray magnetic field where the degree of coupling is controlled by the tuning field, B_0 . The quantum point contact current, I_{QPC} , is used to measure the charge state of the QDs.

mechanical resonator. Furthermore, the effects of the hyperfine interaction on the electron spin states and the corresponding line width of the proposed measurement is also theoretically investigated.

II. DEVICE GEOMETRY AND PARAMETERS

A schematic of the proposed coupled nano-mechanical resonator DD system is shown in fig. 1. A GaAs/AlGaAs nano-mechanical beam of length $2 \mu\text{m}$, width 500 nm and thickness 200 nm is located a distance, d_0 , from the mesa on which the DDs reside. The natural frequency for a resonator of these dimensions is expected to be more than 200 MHz and peak displacement, at the centre of the beam, before the onset of non-linearity of $\sim 5 \text{ nm}$ assuming that the resonator can be driven hard enough with a routinely achievable quality factor of 10^4 .²¹ The double dots are defined using electrostatic gates on the surface of the heterostructure where the 2DEG is located typically 100 nm below the surface²².

The resonator is coupled to the DDs magnetically by placing a Co micro-magnet on the resonator as depicted in fig. 1, with, $\mu_0 M = 1.8 \text{ T}$, where μ_0 and M are the permeability of free space and magnetization of Co respectively. The Co micro-magnet has a length 500 nm ,

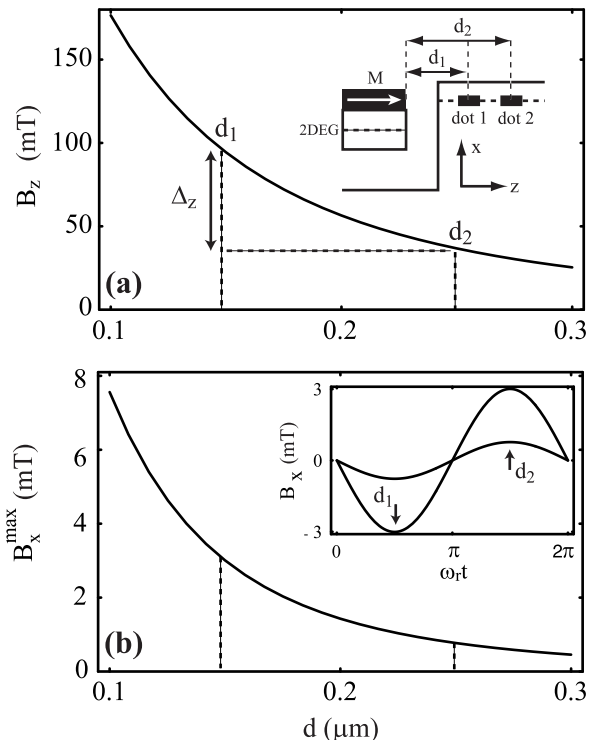


FIG. 2: (a) The profile of the in-plane (Zeeman) magnetic field, B_z , near the nano-mechanical resonator with external tuning field, $B_0 = 0 \text{ T}$ where d_1 and d_2 mark the positions of the left and right quantum dots respectively. The inset shows the cross-section of the proposed system. The position of the micro-magnet is in the same plane as the 2DEG in the mesa on which the double QDs are located. This alignment is achieved by piezoelectrically flexing the beam with the application of DC voltage to the gate defined on the mechanical oscillator and is discussed in detail below. (b) The profile of the transverse magnetic field, B_x^{max} , whilst the resonator is at maximum deflection (5 nm). The inset shows the time dependence of the ESR field at the positions of the quantum dots whilst the mechanical element is at resonance.

width 200 nm and thickness 100 nm and is engineered so that the magnetization vector remains parallel to the easy axis for small values ($\sim 50 \text{ mT}$) of the external tuning field, B_0 . The left and right dots are located a distance, $d_1 = 150 \text{ nm}$ and $d_2 = 250 \text{ nm}$, from the mechanical resonator respectively. Under these conditions, with the nano-mechanical beam at resonance, the total field including the external tuning field is of the form, $B = (B_0 + B_{zn} + \delta B_{zn} \sin(\omega_r t))\hat{z} - B_{xn} \sin(\omega_r t)\hat{x}$. The stray field of the Co micro-magnet has been calculated analogously to the method outlined in ref.²³. The in-plane (Zeeman) magnetic field, B_z , arising from the above described magnetic element is shown in fig. 2a. At the QD locations, the in-plane magnetic field at the left (right) dot is, $B_{z1(2)} = 94 \text{ mT}$ (36 mT). The in-plane component of the magnetic field exhibits almost no temporal dependence ($\delta B_{zn} \ll B_{zn}$) even though the field originates from the magnetic element placed on the

resonator because the beam oscillation is much smaller than the thickness of the micro-magnet. The proximity of the magnetic element to the DDs produces a strong in-plane field gradient of order, $(B_{z1} - B_{z2})/(d_1 - d_2) \sim 0.6 \text{ T}/\mu\text{m}$ which allows the nano-mechanical oscillator to addressably couple to the electron spin in either quantum dot as discussed below. The spatial dependence of the transverse magnetic field, B_x^{max} , whilst the beam is at maximum deflection is shown in fig. 2b. In the inset of fig. 2b, the time dependence of the transverse magnetic field, B_x , at the locations of the DDs whilst the beam is at resonance is shown. The amplitude of this field at the location of the left (right) dot is $\sim 3.0 \text{ mT}$ (0.8 mT) which is more than sufficient to flip the electron spin in either dot via ESR. As can be seen from fig. 2a and b, the parameter, d_0 , is of critical importance as this governs the degree to which the DDs couple to the resonator via the magnetic element.

A. Hamiltonian

For two-electron QDs, the relevant spin states are the spin singlet and triplet states of the (1,1) charge state ($|S\rangle, |T_0\rangle, |T_+\rangle, |T_-\rangle$) and the spin singlet of the (0,2) charge state ($|(0,2)S\rangle$) where the label (m,n) refers to the number of electrons confined on the left and right dots²⁴. In the presence of finite interdot tunnelling, T , the (1,1) and (0,2) singlets are coupled allowing electrons to be moved between dots when the detuning parameter, ϵ , is varied (by pulsing the QD gate voltages). The energy, $\Delta_z = g\mu_B(B_{z1} - B_{z2})/2$, couples the $|S\rangle$ and $|T_0\rangle$ states whilst $|T_+\rangle$ and $|T_-\rangle$ remain eigenstates with Zeeman energy, $\pm E_Z = \pm g\mu_B(B_{z1} + B_{z2} + 2B_0)/2$, where, g , is the electron g-factor ($|g| = 0.44$ for GaAs) and, μ_B , is the Bohr magneton. For the stationary resonator, the Hamiltonian describing the two electron states in the presence of the above described in-plane in-homogeneous magnetic field in the $\{|(0,2)S\rangle, |S\rangle, |T_0\rangle, |T_+\rangle, |T_-\rangle\}$ basis is

$$H = \begin{bmatrix} -\epsilon & \sqrt{2}T & 0 & 0 & 0 \\ \sqrt{2}T & 0 & -\Delta_z & 0 & 0 \\ 0 & -\Delta_z & 0 & 0 & 0 \\ 0 & 0 & 0 & -E_Z & 0 \\ 0 & 0 & 0 & 0 & E_Z \end{bmatrix}. \quad (1)$$

In fig. 3a, the eigenenergies of H are plotted as the detuning is swept between the (1,1) and (0,2) charge states across the degeneracy point ($\epsilon = 0$). For large positive detuning, the ground state is $|(0,2)S\rangle$. Close to $\epsilon = 0$, T and Δ_z mix the $|(0,2)S\rangle$, $|S\rangle$ and $|T_0\rangle$ states. For large negative ϵ , $|(0,2)S\rangle$ uncouples from $|S\rangle$ and $|T_0\rangle$ to become the highest energy state. In the absence of a field gradient ($\Delta_z = 0$), $|S\rangle$ and $|T_0\rangle$ would also be eigenstates with splitting equal to the exchange energy, $J \approx T^2/\epsilon$. However, because $\Delta_z \gg J$, the actual eigenstates are the superpositions, $(|S\rangle \pm |T_0\rangle)/\sqrt{2}$, which correspond to

the states $|\uparrow\downarrow\rangle$ (spin up and spin down at the left and right QDs respectively) and $|\downarrow\uparrow\rangle$ respectively. Moreover, the field gradient in the regime of large negative detuning results in asymmetric separation of $|T_+\rangle$ and $|T_-\rangle$ states about $|\uparrow\downarrow\rangle$ where the energetic separation between the $|\uparrow\downarrow\rangle$ and $|T_+\rangle = |\uparrow\uparrow\rangle$ states is, $\Sigma_{z2} = g\mu_B(B_0 + B_{z2})$, the Zeeman energy of the right spin.

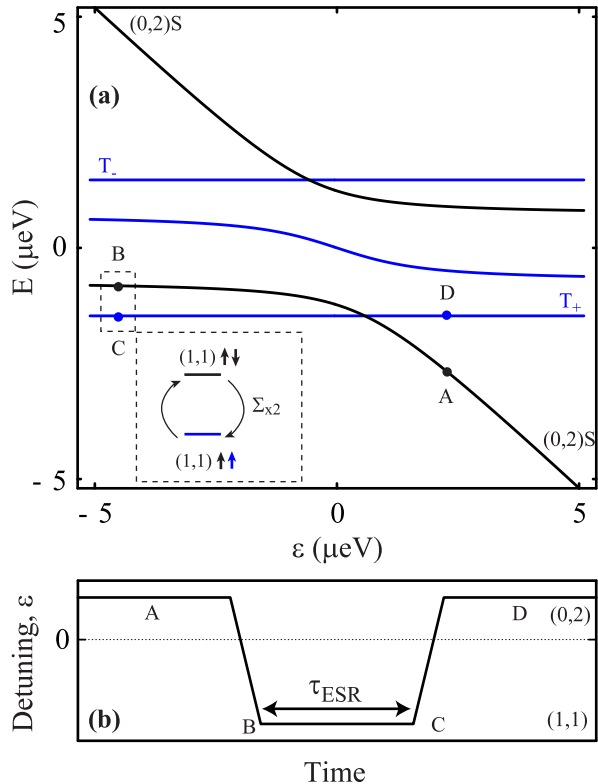


FIG. 3: (a) (colour on-line) The two-electron spin states as a function of detuning energy with interdot tunnelling, $\sqrt{2}T = 1 \mu\text{eV}$ with the external tuning field set to zero. At large negative detuning, the transverse ESR field (B_{x2}) resonantly couples the $|\uparrow\downarrow\rangle$ and $|T_+\rangle$ states (blue line) when the condition, $g\mu_B(B_{z2} + B_0) = \hbar\omega_r$, is satisfied. (b) The pulse sequence consisting of preparation in the $|(0,2)S\rangle$ (A), resonant coupling of the $|\uparrow\downarrow\rangle$ and $|T_+\rangle$ states for time, τ_{ESR} , (B \rightarrow C) and readout (D) steps. For, $\tau_{\text{ESR}} = \tau_\pi$, the final state at point (D) is the triplet $|T_+\rangle$.

III. SPIN ISOLATION AND ESR

The nano-mechanical resonator can be used to manipulate the electron spin states in the DDs as follows. The resonator is excited at its natural frequency corresponding to an energy, $\hbar\omega_r$, the equivalent magnetic field, $\hbar\omega_r/g\mu_B$ is designed to be much greater than GaAs hyperfine magnetic field, $B_N \sim 1 \text{ mT}$. The in-plane tuning magnetic field is then used to adjust the Zeeman spin

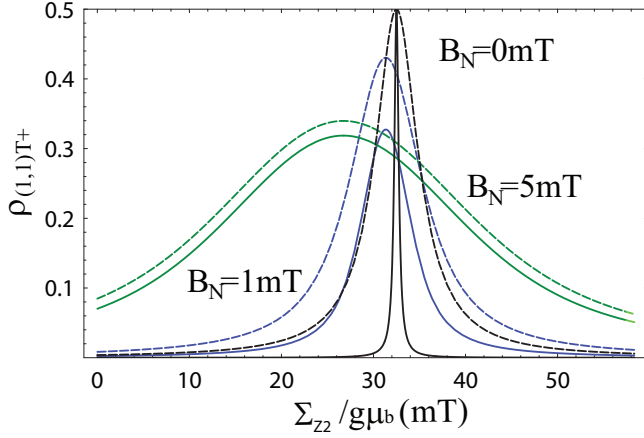


FIG. 4: The expected QPC measurement for the occupation of the $|1, 1\rangle T_+$ state as a function of the field, $\Sigma_{z2}/g\mu_B$, for long ESR mixing time, τ_{ESR} , when the right QD is resonantly coupled to the mechanical element. The resolution of the ESR peak is reduced and broadened by the increasingly strong nuclear field. The range of fields presented here are $\langle B_N \rangle = 0, 1, 5$ mT, with the expected hyperfine field in GaAs being 1mT. The solid lines represent $Q = 10^4$ while the dashed lines represent $Q = 10^5$, illustrating the inverse dependance of the QPC line shape on the quality factor of the resonator. Here the incoherent γ process is negligibly small.

splitting to couple the right QD and the mechanical element by setting $\Sigma_{z2} = \hbar\omega_r$. That is, a tuning field corresponding to the energetic difference between the Zeeman spin splitting at the right QD and the mechanical oscillator results in resonant coupling. For a 200 MHz resonator with the above values for the in-plane magnetic field, the tuning field will be -3.5 mT. With the mechanical element at resonance, the $|(0, 2)S\rangle$ state is prepared (A) which is then separated into the $|\uparrow\downarrow\rangle$ state by the in-plane magnetic field gradient between the two QDs and by using rapid adiabatic passage to change ϵ from a positive to a negative value (A \rightarrow B)¹⁶. With the right QD resonantly coupled to the resonator, the transverse ESR magnetic field couples only the $|\uparrow\downarrow\rangle$ and $|T_+\rangle$ states at a rate proportional to $\Sigma_{x2} = g\mu_B B_{x2}$. The left spin is unaffected by the ESR field due to the large difference in Zeeman field between the QDs. Assuming an infinite quality factor, the Hamiltonian in these conditions is

$$H_{ESR} = -\Sigma_{z2}\sigma_{z2}/2 + \Sigma_{x2}(\omega_r, \omega_d, Q)\sin(\omega_d t)\sigma_{x2}/2, \quad (2)$$

where $\sigma_{n2} = (\sigma_{x2}, \sigma_{y2}, \sigma_{z2})$ are the Pauli matrices of the spin located in the right QD, ω_r is the natural frequency of the resonator, and ω_d is the driving frequency of the resonator. The magnitude of the Σ_{x2} field changes as a function of Q , the quality factor, and ω_d , according to its proportionality to the displacement of the resonator

$$\Sigma_{x2}(\omega_r, \omega_d, Q) = \frac{C}{\sqrt{(\omega_r^2 - \omega_d^2)^2 + 4\omega_r^2\omega_d^2/(Q^2)}}, \quad (3)$$

where C is a proportionality constant. For later use we define $\delta\omega = \omega_r^2 - \omega_d^2$.

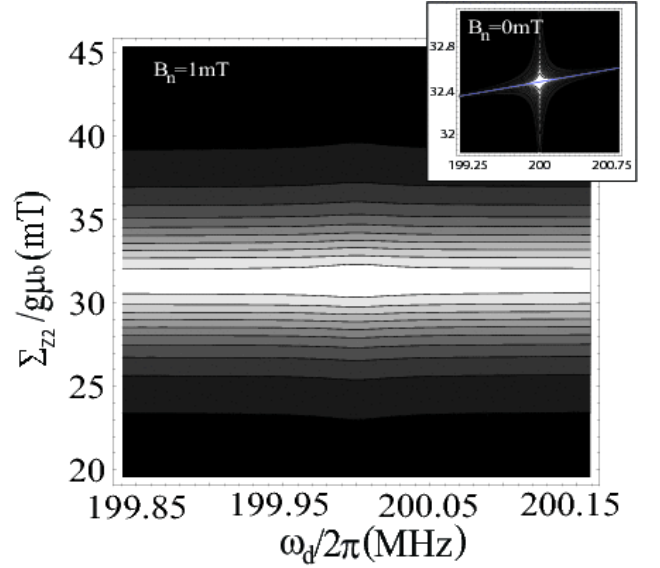


FIG. 5: A contour plot of the expected QPC measurement for the occupation of the $|1, 1\rangle T_+$ state as a function of the field, $\Sigma_{z2}/g\mu_B$, and the driving frequency of the resonator ω_d , for long ESR mixing time, τ_{ESR} , and hyperfine interaction $\langle B_N \rangle = 1$ mT. The inset shows the same response for the zero hyperfine interaction. The horizontal arm of the ‘star’ is defined by $\Sigma_{z2}/\hbar - \omega_d = 0$, as illustrated by the superimposed line in the inset. When the hyperfine interaction is on, the horizontal arm is broadened considerably, with only a small exaggerated response at the $\omega_r = \omega_d$ point. Here, white is maximum (0.42 for the main figure, ≈ 0.5 for the inset), black is minimum.

The coupled system is held in this state for time, τ_{ESR} , until steady state has been achieved (B \rightarrow C). After manipulation, rapid adiabatic passage is used to change ϵ from negative to positive values for charge sensing measurement via the quantum point contact, QPC (C \rightarrow D). The $|(1, 1)T_+\rangle$ state remains in the spin-blocked configuration whereas the $|\uparrow\downarrow\rangle$ tunnels directly to $|(0, 2)S\rangle$. A schematic of this pulse sequence is shown in fig. 3b. After manipulation, the spin state is a mixture of $|(0, 2)S\rangle$ and $|(1, 1)T_+\rangle$ states (at point D). In this condition, the QPC current, I_{QPC} , will be a mixture of the corresponding (0,2) and (1,1) charge states. At off resonance, the spin configuration at (D) will be $|(0, 2)S\rangle$ with (0,2) QPC signal. Therefore, by sweeping the tuning field across resonance, a peak in the I_{QPC} is expected.

IV. MASTER EQUATION OF ESR HAMILTONIAN

The response of the QPC can be modeled using a master equation model for H_{ESR} . To robustly model the coupled system, the various mechanisms by which the electron spins can decohere are considered. The $|(0, 2)S\rangle$ is initialized at point A in the schematic of the pulse sequence shown in fig. 3b. On experimental time scales,

this state is highly robust and no spin dephasing takes place. Concurrently the mechanical element is at resonance and thermal fluctuations in its motion can result in the ESR field smearing out i.e. the time dependence of the ESR field shown in the inset of fig. 2b will result in small amplitude oscillations being super-imposed on the sinusoidal ESR response. However, the amplitude of these thermal fluctuations can readily be extracted from the equipartition theorem and for the operating temperature of this experiment (~ 50 mK) the thermal amplitude is expected to be ~ 0.1 pm which is more than 4 orders of magnitude less than the amplitude of the beam. Therefore, spin dephasing due to thermal noise in the mechanical element is negligible. Furthermore, the Curie temperature of the Co micro-magnet is 1394 K which is much greater than the operating temperature of the proposed experiment. Hence spin dephasing due to fluctuations in the ferromagnetic properties of Co are again negligible. In general electrical noise (the detuning parameter, ϵ , is varied by pulsing the voltages of the QD gates) induced fluctuations in the exchange energy, J (via Δ and T noise) lead to extra mixing between the $|(0, 2)S\rangle$, $|S\rangle$ and $|T_0\rangle$ states. However, because the spins are manipulated at large detuning, gate voltage noise can be neglected because $dJ/d\Delta \sim 0$ in this regime, i.e. the states are to first order insensitive to electrical noise. As demonstrated in ref.²⁵, spin-orbit coupling, which is an extra decoherence channel can be neglected in GaAs quantum dot system

for the proposed experimental timescales. The remaining main decoherence mechanism for the electron spin is the Hyperfine interaction with nuclear spins within the quantum dots²⁶. We ignore the hyperfine interaction for the electron in the left dot by assuming the mean nuclear magnetic field is much smaller than the Zeeman splitting, thus the spin state is not flipped. In addition, because of the large energy difference between the two dots, we can ignore inelastic singlet-singlet transitions.

Under these conditions, the master equation describing the spin states of the electron in the right dot is,

$$\hbar \frac{d\rho(t)}{dt} = -i[H_{ESR} + H_N, \rho(t)] + L[\rho(t)], \quad (4)$$

where $H_N = -g \cdot \mu_B (B_N \cdot \sigma_2)$ is the hyperfine interaction and $L[\rho(t)]$ describes the incoherent Markovian spin relaxation at rate γ . We reach the steady state solution by taking $t \rightarrow \infty$, $\frac{d\rho(t)}{dt} = 0$, and thus inverting to find $\rho(t \rightarrow \infty) = [-i\hbar[H_{ESR} + H_N, \rho(t)] + L]^{-1}$. Assuming the rotating wave approximation, we are able to obtain an analytical solution for the occupation of the $|(1, 1)T_+\rangle$ and $|(0, 2)S\rangle$ states.

For static hyperfine nuclear fields B_N , the steady state of the density matrix elements for the diagonal $|(1, 1)T_+\rangle$, $|(0, 2)S\rangle$, and the off-diagonal $\langle(1, 1)T_+|\rho|(0, 2)S\rangle$, states are (omitting the notation $t \rightarrow \infty$),

$$\rho_{(1,1)T_+} = \frac{16B_{Y,N}^2 + (4B_{X,N} + \Sigma_{x2})^2}{32(B_{X,N}^2 + B_{Y,N}^2 + 2B_{Z,N}^2) + 32\Sigma_{x2}B_{X,N} + 64\hbar B_{Z,N}\Delta\omega + 2\Sigma_{x2}^2 + \hbar^2 16\Delta\omega^2 + 4\hbar^2\gamma^2} \quad (5)$$

$$\rho_{(0,2)S} = 1 - \rho_{(1,1)T_+} \quad (6)$$

$$\rho_{(1,1)T_+, (0,2)S} = \frac{(4(B_{X,N} - iB_{Y,N}) + \Sigma_{x2})(4B_{Z,N} + 2\hbar\Delta\omega - i\hbar\gamma)}{16(B_{X,N}^2 + B_{Y,N}^2 + 2B_{Z,N}^2) + 16\Sigma_{x2}B_{X,N} + 32\hbar B_{Z,N}\Delta\omega + \Sigma_{x2}^2 + \hbar^2 8\Delta\omega^2 + 2\hbar^2\gamma^2}. \quad (7)$$

where $\Delta\omega = \Sigma_{z2}/\hbar - \omega_d$ is the Rabi frequency, γ is a phenomenological damping of the spin state, and $B_{i,N}$ is the nuclear field in the i th direction. The off-diagonal term is in the rotating frame. We assume that the nuclear field is static on the \hbar/Σ_{x2} and $1/\gamma_1$ time scales, but is fast on the time scale of collating a clear QPC measurement. Thus, in the data presented in fig. 4, we integrate over a normal distribution of possible nuclear spin orientations²⁷ with mean value $\langle B_N \rangle = \sqrt{3}\langle B_{i,N} \rangle$, and a standard deviation of $\sqrt{2}\langle B_N \rangle$, so

$$\langle \rho_{(1,1)T_+} \rangle_{B_N} = \int_{-\infty}^{\infty} \rho_{(1,1)T_+} \prod_{i=x,y,z} \frac{e^{\left[\frac{-(B_{i,N}^2 - \langle B_{i,N}^2 \rangle)^2}{4\langle B_{i,N}^2 \rangle} \right]}}{(2\langle B_{i,N} \rangle \sqrt{\pi})} dB_{i,N}. \quad (8)$$

Consequently, $\langle B_N \rangle$ is the important quantity in deter-

mining the affect of the nuclear field on the ESR measurement. In fig. 4, the effects of the hyperfine coupling on the QPC measurement are shown. For $\langle B_N \rangle < \Sigma_{x2}$ the on resonance response of the QPC is clearly visible. For $\langle B_{0,N} \geq \Sigma_{x2} \rangle$ the on resonance peak becomes smeared out and eventually obliterated.

V. ESR LINE WIDTH AND RESONATOR QUALITY FACTOR

Ignoring the hyperfine interaction and the stochastic decoherence rate of the spin ($\gamma = 0$), we can see very clearly how the line width of the ESR response depends on the Quality factor of the resonator. The ESR response

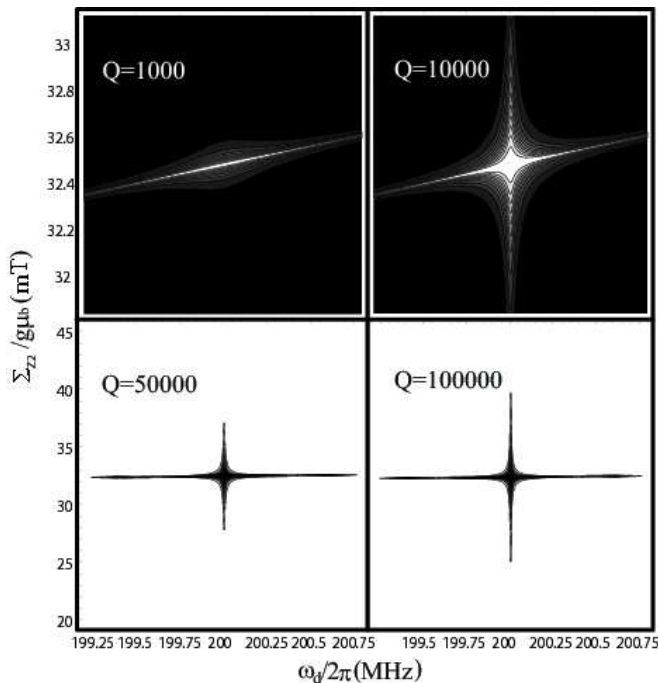


FIG. 6: Contour plots of the expected QPC measurement for the occupation of the $|1, 1\rangle_{T_+}$ state as a function of the field, $\Sigma_{z2}/g\mu_B$, and the driving frequency of the resonator ω_d , for zero hyperfine interaction, and a range of Q factors. Changing the Q factor alters the range of the vertical arm ($\omega_d - \omega_r = 0$) of the star. In the top two figures, white is maximum. In the bottom two figures, black is maximum (for clarity).

is,

$$\rho_{(1,1)T_+} = \frac{1}{2(1 + \frac{2\hbar^2}{\Sigma_{x2}^2} \Delta\omega^2)}. \quad (9)$$

However, as mentioned earlier, the field Σ_{x2} is both Q and ω_d dependant. This gives the following Lorentzian form with two maxima,

$$\rho_{(1,1)T_+} = \frac{1}{2(1 + \frac{32\hbar^2\omega_d^2\omega_r^2}{Q^2C^2}\Delta\omega^2 + \frac{8\hbar^2\Delta\omega^2}{C^2}\delta\omega^2)}. \quad (10)$$

Thus the line width of the ESR response, obtained by sweeping the tuning field, is

$$\gamma^{ESR} = \frac{QC}{\hbar\sqrt{8(4\omega_d^2\omega_r^2 + Q^2(\omega_d^2 - \omega_r^2)^2)}}. \quad (11)$$

where C again is the constant defined by properties of the resonator (see Eq. [3]). When the resonator is driven at resonance $\omega_d = \omega_r$, the ESR line width is $\gamma_L \approx Q$, the inverse of the resonators own line width, Eq. [3]. This can be understood by the fact that the reduced motion of the resonator, because of a lower Quality factor, implies a reduced maximum Σ_{x2} field, which in turn reduces the steady state probability for the spin to be in the $|(1, 1)T_+\rangle$ state when the Rabi tuning $\Delta\omega$ is off-resonance. Fig. 6 illustrates the effect of changing Q on the QPC measurement.

In addition, for large detuning of the resonator driving frequency from the natural frequency $\delta\omega = \omega_d^2 - \omega_r^2$, we find that $\gamma_L \approx 1/\sqrt{(\omega_d^2 - \omega_r^2)}$. Hence the $\Delta\omega$ peak becomes very sharply defined and almost independent of the quality factor. Thus the transduction of the resonator motion by ESR is advantageous because it allows us to read out both the quality factor Q and intrinsic properties of the resonator via the constant C . Furthermore, for large detuning $\omega_d^2 - \omega_r^2$, the spin rotation can be performed with a very narrow line width.

Alternatively, by fixing the tuning field at $B_0 = \hbar\omega_r/g\mu_B - B_{z2}$ (B_{z2} can be measured in principle by DD spectroscopy²⁸) and sweeping the frequency of the mechanical oscillator about the resonance point, $\delta\omega = \Delta\omega = 0$, a peak in I_{QPC} is again seen. But now the corresponding line shape is the convoluted response of the nano-mechanical oscillator and the two-electron system. If the tuning field is moved away from the $\omega_r/g\mu_B$ point, both maxima in the double Lorentzian are visible. In this case, the two peaks both have a ω_d dependant line shape, which dominates over the Q dependence.

Additionally, moving beyond the steady state, the mechanical resonator provides a local ESR field which enables the electron spin states to be manipulated. For example, by modulating the waiting time (B→C) to provide a π pulse so that, $\tau_{ESR} = \tau_\pi = 2\pi\hbar/\Sigma_{x2} = 0.2 \mu s$, then the final state at readout is the triplet $|T_+\rangle$. By employing a larger tuning field, the states $|\uparrow\downarrow\rangle$ and $|T_-\rangle$ can also be resonantly coupled so that the spin of the left dot is flipped given the tuning field is less than the Co switching field so that the magnetisation does not reverse.

In the above described coupled system, actuation of the mechanical element is achieved via the piezoelectric effect between the top gate defined over one of the clamping points of the beam and the shallow buried 2DEG²⁹. The mechanical resonance is then excited by applying an AC voltage to the top gate at the mechanical resonance frequency. Crucial to the success of this scheme is the in-plane alignment of the micro-magnet and the shallow buried 2DEG on the mesa on which the DQDs are defined. This can be achieved by applying a DC voltage to the top gate on the mechanical element which will induce a static deflection of the mechanical beam enabling alignment to be achieved as visualised in the inset of fig. 2a. Simultaneously a small AC modulation will drive the beam to mechanical resonance.

VI. CONCLUSIONS

A two-level system realized in a two-electron double quantum dot is a highly sensitive quantum detector. Magnetically coupling the double quantum dots to a high frequency nano-mechanical resonator will allow the displacements of the resonator to be detected. Tuning the Larmor frequency to match the resonators natural frequency, the electron spin in one of the dots can be flipped.

By simultaneously measuring the charge state of the double quantum dots, this transition can be detected thus enabling the natural frequency of the mechanical resonator to be determined.

The authors NL, IM and MP-L have contributed equally to this manuscript. The authors also acknowledge A. Blais for useful discussions and for critically reading the manuscript. S. Camou, S. Etaki, C. Buizert

and H. Inagaki are thanked for their help and encouragement. We acknowledge financial support from the Grant-in-Aid for Scientific Research A (No. 40302799), the Special Coordination Funds for Promoting Science and Technology, MEXT, SORST-JST, DARPA grant no. DAAD19-01-1-0659 of the QuIST program and JSPS KAKENHI(16206003) and JSPS grant 17-05761.

-
- * Electronic address: lambert@asone.c.u-tokyo.ac.jp
- ¹ H. G. Craighead, *Science* **290**, 1532 (2000).
 - ² A. Cho, *Science* **299**, 36 (2003).
 - ³ M. Roukes, *Phys. World* **14**, 25 (2001).
 - ⁴ R. G. Knobel and A. N. Cleland, *Nature* **424**, 291 (2003).
 - ⁵ M. D. LaHaye, O. Buu, B. Camarota, and K. C. Schwab, *Science* **304**, 74 (2004).
 - ⁶ A. Naik, O. Buu, M. D. LaHaye, A. D. Armour, A. A. Clerk, M. P. Blencowe, and K. C. Schwab, *Nature* **443**, 193 (2006).
 - ⁷ M. R. Geller and A. N. Cleland, *Phys. Rev. A* **71**, 032311 (2005).
 - ⁸ F. Xue, Y. D. Wang, C. P. Sun, H. Yamaguchi, and K. Semba, [arXiv:cond-mat/0607180v1](https://arxiv.org/abs/cond-mat/0607180v1).
 - ⁹ S. M. Carr, W. E. Lawrence, and M. N. Wybourne, *Phys. Rev. B* **64**, 220101 (2001).
 - ¹⁰ S. Savel'ev, X. Hu, and F. Nori, [arXiv:cond-mat/0412521](https://arxiv.org/abs/cond-mat/0412521).
 - ¹¹ A. Wallraff, D. Schuster, A. Blais, L. Frunzio, R. S. Huang, J. Majer, S. Kumar, S. M. Girvin, and R. J. Schoelkopf, *Nature* **431**, 162 (2004).
 - ¹² R. C. Ashoori, *Nature* **379**, 413 (1996).
 - ¹³ S. Tarucha, D. G. Austing, T. Honda, R. J. van der Hage, and L. P. Kouwenhoven, *Phys. Rev. Lett.* **77**, 3613 (1996).
 - ¹⁴ M. Ciorga, A. S. Sachrajda, P. Hawrylak, C. Gould, P. Zawadzki, S. Jullian, Y. Feng, and Z. Wasilewski, *Phys. Rev. B* **61**, R16315 (2000).
 - ¹⁵ D. Loss and D. P. DiVincenzo, *Phys. Rev. A* **57**, 120 (1998).
 - ¹⁶ J. Petta, A. Johnson, J. Taylor, E. Laird, A. Yacoby, M. Lukin, C. Marcus, M. P. Hanson, and A. Gossard, *Science* **309**, 2180 (2005).
 - ¹⁷ F. H. L. Koppens, C. Buizert, K. J. Tielrooij, I. T. Vink, K. C. Nowack, T. Meunier, L. P. Kouwenhoven, and L. M. K. Vandersypen, *Nature* **442**, 766 (2006).
 - ¹⁸ F. Xue, L. Zhong, Y. Li, and C. P. Sun, [arXiv:quant-ph/0602219v2](https://arxiv.org/abs/quant-ph/0602219v2).
 - ¹⁹ D. Rugar, R. Budakian, H. J. Mamin, and B. W. Chui, *Nature* **430**, 329 (2004).
 - ²⁰ J. M. Elzerman, R. Hanson, L. H. W. van Beveren, B. Witkamp, L. M. K. Vandersypen, and L. P. Kouwenhoven, *Nature* **430**, 431 (2004).
 - ²¹ At large oscillation amplitudes bi-stability occurs where the effective spring constant of the beam increases and the resonance peak migrates to higher frequencies simultaneously developing asymmetry at the expense of quality factor.
 - ²² J. M. Elzerman, R. Hanson, J. S. Greidanus, L. H. W. van Beveren, S. D. Franceschi, L. M. K. Vandersypen, S. Tarucha, and L. P. Kouwenhoven, *Phys. Rev. B* **67**, 161308 (2003).
 - ²³ M. Pioro-Ladrière, Y. Tokura, T. Obata, T. Kubo, and S. Tarucha, *Appl. Phys. Lett.* **90**, 024105 (2007).
 - ²⁴ J. M. Taylor, H.-A. Engel, W. Ur, A. Yacoby, C. M. Marcus, P. Zoller, and M. Lukin, *Nature Physics* **1**, 177 (2005).
 - ²⁵ A. V. Khaetskii and Y. V. Nazarov, *Phys. Rev. B* **64**, 125316 (2001).
 - ²⁶ W. A. Coish and D. Loss, *Phys. Rev. B* **72**, 125337 (2005).
 - ²⁷ F. H. L. Koppens, C. Buizert, I. T. Vink, K. C. Nowack, T. Meunier, L. P. Kouwenhoven, and L. M. K. Vandersypen, *J. Appl. Phys.* **101**, 081706 (2007).
 - ²⁸ S. D. Barrett and T. M. Stace, *Phys. Rev. Lett.* **96**, 017405 (2006).
 - ²⁹ I. Mahboob, S. Miyashita, and H. Yamaguchi, unpublished.